Euro PM2015 – Non-Ferrous and Special Materials

Manuscript refereed by Professor Elena Gordo (Madrid University Carlos III, Spain)

Effects of Build Orientation Induced Surface Modifications on the In-Vitro Biocompatibility of Electron Beam Melted Ti-6Al-4V

Alfred T. Sidambe[1,], Iain Todd[2], Paul V. Hatton[3]*

1. *JRI Orthopaedics, 35A Business Park, 18 Churchill Way, SHEFFIELD, S35 2PY, UK; E-Mail: a.t.sidambe@gmail.com*
2. *Materials Science and Engineering Dept., University of Sheffield, Mappin Street, SHEFFIELD, S1 3JD UK; E-Mail: i.todd@sheffield.ac.uk*
3. *Bioengineering & Health Technologies Group, School of Clinical Dentistry, University of Sheffield, 19 Claremont Crescent, SHEFFIELD, S10 2TA UK; E-Mail: paul.hatton@sheffield.ac.uk*

* *Author to whom correspondence should be addressed; E-Mail: a.t.sidambe@gmail.com; Tel.: + 44 114 345 3200; Fax: + 44 114 257 3254.*

Abstract: Titanium and its alloys may be processed via additive manufacturing techniques such as Electron Beam Melting (EBM). This field is receiving increased attention from various manufacturing sectors including the medical devices sector. While the economic and engineering potential of EBM for the manufacture of musculo-skeletal implants is clear, the impact on the biocompatibility of the materials has been less investigated. In this study, effects of build orientation induced surface modifications on the in-vitro biocompatibility of the EBM Ti6Al4V alloy were investigated. The study assessed the suitability of three different Ti6Al4V surfaces produced via the EBM process as variables for proliferation and attachment of mouse fibroblast L929 cells. The three different surface topographies were obtained by orienting the builds in vertical, horizontal and inclined (55°) orientations in the EBM build chamber. The mouse fibroblasts were cultured *in vitro* on the Ti6Al4V alloy discs with three different surface finishes. Cell viability studies, fluorescent microscopy as well as scanning electron micrographs were used to assess the L929 cell attachment and proliferation. After 2 and 8 days of incubation there was a higher vitality and proliferation of L929 cells on the vertical and inclined surfaces (R_a = 38 µm and 46 µm respectively) than on the horizontal surfaces (R_a = 18 µm). On the vertical and inclined samples, the cells spread over a wider area whereas on the horizontal samples cell spread was affected by the topographical features. The results showed that that the implants produced by EBM meet basic biocompatibility requirements and also showed that build orientation of titanium during EBM can produce surfaces with different characteristics and these can affect cell growth.

Keywords: Ti6Al4V; Titanium; Additive Manufacturing; Biocompatibility; 3-D Printing; Cytotoxicity; Implants; L929 fibroblasts; cell culture.

1. Introduction

Titanium (Ti) and titanium alloys are an excellent choice for biomedical applications because they exhibit a high specific strength [1] [2]. Ti is also considered to be biocompatible because it has a low electrical conductivity, a high resistance to corrosion, a thermodynamic state at pH values of the human or animal body, a low formation of ions in wet conditions, and an oxide isoelectric point of 5–6 [3]. Ti alloys are used in biomedical implant devices which replace damaged hard tissue. Some examples of Ti uses in biomedical applications are dental and orthopaedic implants, artificial hearts, pacemakers, artificial knee joints, bone plates, cardiac valve prostheses, screws for fracture fixation and artificial hip joints [4]. Titanium and titanium alloys have therefore been used widely as biomedical implant materials since the early 1970s and the implants have been available as machined and cast components. The alloys that are preferred for the fabrication of titanium implants are commercially pure titanium (CP-Ti) and titanium alloy Ti6Al4V (Ti-64). Out of the two, Ti-64 is preferred in many applications because it offers an excellent combination of high strength, excellent corrosion resistance and is easier to process [5].

The widespread use of titanium and it alloys has been limited by high cost due to the multi-step Kroll extraction process of the Ti raw material [6]. Titanium production is also hampered by the high cost in traditional manufacturing processes, and poor workability for complex shape production. This has led to numerous investigations of various potentially lower-cost processes which involve powder

metallurgy [6]. Powder metallurgy routes of titanium processing have emerged as techniques that can minimise the cost of production, particularly for complex shapes and for implant fabrication because they enable production of near net shape components [3]. The various routes that utilise powder metallurgy have been reviewed by Froes [6] [7] and Sidambe [3]. Advanced powder bed manufacturing routes such as additive layer manufacturing (ALM) offer design flexibility for fabricating products that have complicated shapes with a very high accuracy. ALM is distinct from traditional machining techniques, which mostly rely on the removal of material by methods such as cutting or drilling (subtractive manufacturing) [8]. Thus, ALM is increasingly being employed as a process for fabricating surgical implants including orthopaedic and dental implants. With increasing demand for medical implantation, there is increasing need for implants that offer reliability, adequate mechanical properties and offer unique properties (such as patient specific implants) as well as comfort. ALM is therefore used in the orthopaedic sector to make patient specific, complex, cellular and functional mesh arrays implants or bone substitutes [9] [10] [11].

1.1 Additive Layer Manufacturing

Additive layer manufacturing comprises a cluster of technologies that have emerged in the last two decades. In ALM, objects are created by adding the material one cross-sectional layer at a time [12]. ALM makes use of the additive method to form a three-dimensional (3D) solid object of almost any shape from a computer aided drawing (CAD) model. The geometry of the object is designed onto a CAD file model which is then "sliced numerically" into the layer thickness the machine will build in. It is then transferred to the ALM machine's software and loaded to the ALM machine allowing a file based build to commence. Layers of material are laid down one after the other with each layer corresponding to a different shape. Figure 1 (a) illustrates the flow of data between from CAD file to component in the ALM system [3]. ALM technologies include fused deposition modelling, laser micro-sintering, direct metal laser sintering (DMLS), three-dimensional (3-D) laser cladding, electron beam melting (EBM), and electron beam sintering (EBS) [13] [8]. This study is confined to the EBM technique.

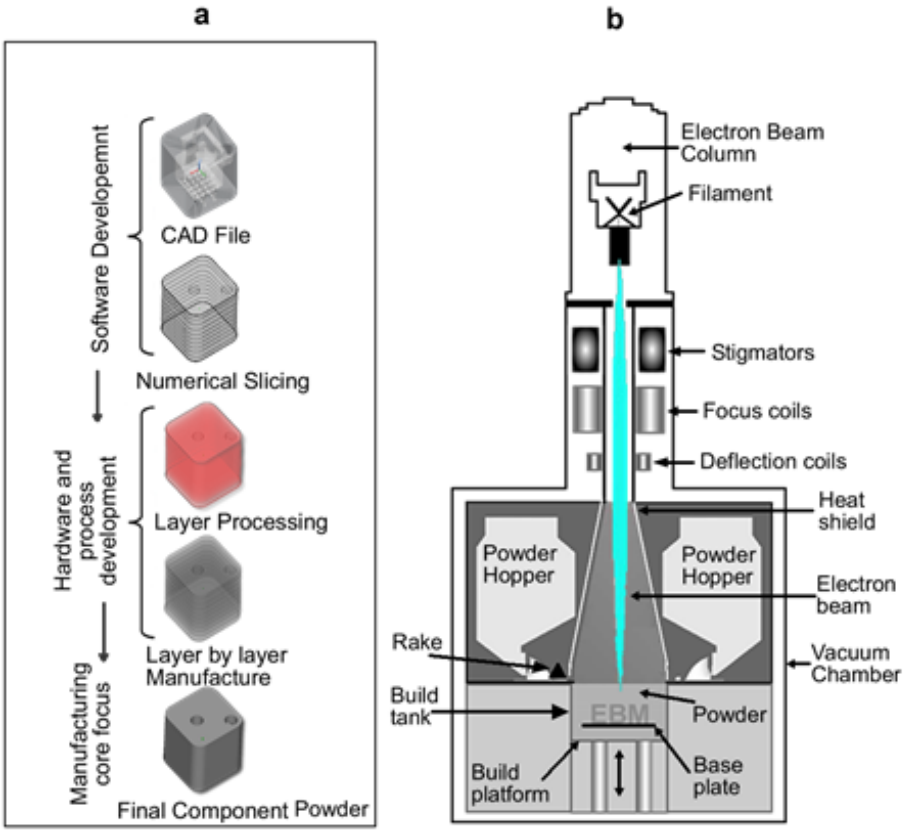

Figure 1**:** Flow of data between from CAD file to component in the ALM system (a) and Schematic drawing of an electron beam melting system [3].

1.1.1 *Electron Beam Melting (EBM)*

Electron beam melting (EBM) is one of the additive manufacturing techniques mainly used for metallic biomaterials. The EBM system manufactures parts by melting the metal powder layer by layer using a magnetically directed electron beam under a high vacuum atmosphere [14]. It is for this reason that EBM is particularly suited for the manufacturing of titanium and titanium alloy implants. EBM allows for the fabrication of titanium implants which promote improved bone regeneration and increased contact area at the interface of implant and tissue- via a larger specific surface area. Figure 1 (b) is a schematic drawing of an electron beam melting system and it shows that the electron beam is generated by filaments (and anodes). The beam is then focused by three lenses onto the build area under a controlled vacuum environment ($<5 \times 10^{-4}$ mbar). During the build, the powder is supplied from the hoppers and spread by the rake on to the top of the build where it is selectively melted by the electron beam as it scans the surface. A component is created by adding new layers of powders over the previous ones repeatedly [11, 15].

Part of the challenges of using EBM in the manufacturing of surgical implants is to optimise the surface finish of the final components. This highly depends on the EBM processing parameters such as beam current, part orientation and powder particle size. It is widely known and accepted that the surface topography of biomedical implants affects the biocompatibility because it influences the cell attachment, proliferation, and differentiation [16]. The performance of biomedical implants and their biocompatibility depends very much on the initial interaction between surfaces of the implants and the biological environment [17]. The development of new processes such as EBM does not typically include biocompatibility testing until the prototype stage is reached. Regulation agencies such as the Food and Drug Administration (FDA) in the USA require biocompatibility testing per ISO 10993 or ASTM F748 prior to device approval [18]. Therefore there is a need to carry out biocompatibility testing in any material or new material processing method [18]. There are a number of studies that have been carried out to determine the biocompatibility of titanium implants manufactured via EBM [17, 19] [20] [10] [21] [22]. The results of the biocompatibility of Ti-64 EBM listed above are varied and they show to a certain extent that EBM of titanium can be adopted for the fabrication of custom orthopaedic implants. However the literature search has not revealed any studies which examine the differences that occur depending on the orientation of the implant in the build chamber and the effect on cell growth.

The aim of this study has been to fabricate and characterise Ti-64 components with differing surface finishes which have been obtained a result of build orientation using the EBM process. Secondly, the effect of the different surface finishes on cell attachment, proliferation and cell morphology has been investigated, *in vitro*. The surfaces and effect on L929 fibroblast cells of the EBM Ti-64 discs were compared to Ti-64 discs manufactured via the metal injection moulding (MIM) process. A MIM surface was selected as a reference for this study in order to differentiate between homogenous and inhomogeneous powder source topographies. More details about the MIM processing of the discs has been reported elsewhere [23]. The study has been carried out because of the implications for the design and clinical applications that manufacturing Ti-64 implants via the EBM process brings.

2. **Materials and Experimental Techniques**

2.1 Titanium discs

Using standard medical grade titanium alloy Ti-64 (ELI) as supplied by Arcam AB, with a nominal particle size range of 45µm to 105µm, the Arcam S12 EBM system (Arcam AB, Molndal, Sweden) was utilised to produce three types of titanium discs (2 mm thick, 10 mm diameter each). Standard melt themes encompassing the beam current, offset focus and scan speed for the Ti-64 powder were used along with a layer thickness of 70µm. Three different surface roughnesses were obtained by orienting the builds in vertical, horizontal and inclined (55°) orientations in the EBM build chamber. Figure 2 (a) shows a CAD illustration of the build orientations of the Ti-64 discs whereas and the manufactured Ti-64 discs showing the different surface finishes are shown in Figure 2 (b). After the parts were manufactured on the EBM machine, powder blasting was used to remove loose metallic particles from the surfaces of the parts. The size of the discs was selected so that they would to fit into the 24-well cell culture plate for the *in vitro* biocompatibility studies.

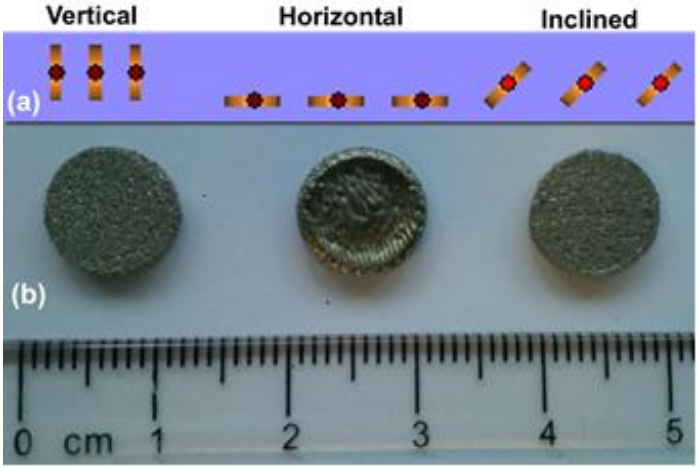

Figure 2: Illustrations of the build orientations of the Ti-64 discs (a) and the manufactured Ti-64 discs showing the different surface finishes

2.2 Surface characteristics

Parameter	Definition
R_a (µm)	Average roughness – the area between the roughness profile and its arithmetic mean line.
R_q (µm)	Root mean square parameter average roughness. (R_q is more sensitive to peaks and valleys and is better for discriminating different types of surfaces).
R_p (µm)	The height of the highest peak in the roughness profile. Mathematically the largest peak deviation of the roughness profile from the mean line within a sampling length.
R_v (µm)	Maximum profile valley depth. Depth of the deepest valley in the roughness profile.
R_t (µm)	The sum of R_p and R_v. Total height of the profile or vertical distance from deepest valley to highest peak.

Table 1: Definitions of the surface roughness parameters that were studied

The characterisation of the surface profiles was carried out using the Contour GT 3D Optical Profiler (Bruker UK Ltd, Coventry, UK). The profiler was used in conjunction with the Vision64™ software. The Contour GT is based on the fundamental science of white light interferometry and is designed to deliver high resolution images and surface measurements. The surface roughness parameters that were characterised in this study, together with their definitions are specified in Table 1 below. Surface characteristics were also studied via SEM using the Inspect-F50 (FEI, Oregon,USA) and Philips XL 20 (Royal Philips Electronic, Eindhoven, The Netherlands) SEM's operated with an accelerating voltage of 20 kV.

2.3 Cell Culture

Prior to biocompatibility testing, all the disc implants were sterilised by rinsing in methylated industrial spirit (IMS, Fisher Scientific, Loughborough, UK), phosphate buffer saline (PBS, pH 7.4) from Sigma-Aldrich, Dorset, UK and distilled water for a total of 15 minutes. Further sterilisation was carried out by steam autoclaving for 30 min at 120°C. Biocompatibility testing was carried out using the L929 fibroblast cells (ATCC, Rockville, MD, USA). The L929 fibroblast cell was selected because it is an established and robust cell line recommended according to ISO 10993-5 standards on *in vitro* cytotoxicity testing [24].

The L929 fibroblast cells were cultured in Dulbecco's Modified Eagle Medium nutrient mixture (DMEM, Fisher Scientific) supplemented with Non-essential amino acids (N.E.A.A) from Lonza, UK, Penicillin Streptomycin (PS), Lglutamin (Sigma-Aldrich), Hepes (Sigma-Aldrich) and 10% Fetal Calf Serum (FCS, Sigma-Adrich). Cells were placed into T75 cell culture flasks and incubated at 37°C and 5% CO_2/Air. $1x10^6$ cell were seeded per T75 flask. Medium was changed every 3 days until the cells were confluent. The cells were harvested and then seeded on the Ti-64 EBM discs as well as on the reference MIM Ti-64 discs which were placed in 24-well cell culture plates. Cells on Ti-64 implant discs

were cultured in the same nutrient mixture as described above and then incubated for 2 and 8 days (n=6). 0.25 x 10^6 L929 cells were seeded per Ti-64 implant disc.

2.3.1 *Cell Viability*

The viability of the L929 cells cultured on Ti-64 discs was carried out using fluorescent and calometric methods. The PrestoBlue® Cell Viability Reagent (Life Technologies, Paisley, UK) was used to detect metabolic activity. PrestoBlue® is a ready to use cell permeable resazurin-based solution that functions as a cell viability indicator by using the reducing power of living cells to quantitatively measure the proliferation of cells [25] . The discs containing cultured cells were washed with PBS and placed into new well plates using sterile tweezers and the assay was performed in the dark because PrestoBlue is light sensitive. A 1:10 dilution of PrestoBlue® in DMEM media was prepared and 2ml of PrestoBlue® was added to each well plate containing a Ti-64 disc specimen. 2ml was added to empty wells as a control measure and then the 24-well plate was placed in the incubator. After 30 minutes and 60 minutes, 200µl of PrestoBlue® was removed from each well and transfered into wells of a 96-well plate in triplicate order. The 96 well plate was then placed in a Tecan plate reader (Tecan, Switzerland) and the fluorescence was read at excitation wavelength of 530nm with 590nm emission wavelength using the Magellan™ data analysis software.

2.3.2 *Cytotoxicity*

The L929 mouse fibroblasts that were cultured in 24-well plates for 2 days on Ti-64 discs were counted using the CytoTox 96® non-radioactive cytotoxicity assay (Promega UK, Southampton, UK). This assay quantitatively measures cellular lactate dehydrogenase (LDH), a stable cytosolic enzyme that is released on cell lysis. LDH oxidises lactate into pyruvate, generating NADH, which is then used to convert a tetrazolium salt into a red formazan product. The amount of colour formed is proportional to the number of lysed cells. A standard curve for determination of cell numbers was constructed using cells seeded at 1.32x10^6 cells/mm. Cells that remained alive by the end of the 2 day experiment were detached and lysed for the release of LDH, which was then measured. LDH activity was analyzed using the cytotoxicity detection kit and sample collection was performed according to the cytotoxicity kit manufacturer's instructions [26]. The absorbance was measured on a Tecan plate reader at 490nm because it is considered proportional to the catalytic activity of LDH.

2.3.3 *Cell morphology*

The cell morphology and spread was analysed using scanning electron microscopy and fluorescent confocal microscopy. The preparation for SEM analysis was carried out on L929 fibroblast cells cultured for 2 and 8 days on the Ti-64 discs. The Ti-64 discs were moved onto new 24 -well plates using sterile tweezers. In order to fix the cells, 3ml of 0.1M cacodylate buffer (buffer) was added to each well plate and left for 5 minutes. Attached cells were fixed with 3% glutaraldehyde in 0.1M cacodylate buffer (Sigma-Aldrich, UK) for 30 minutes at room temperature and then washed three times with buffer. A postfix treatment in 2% osmium tetroxide (Sigma-Aldrich, Dorset, UK) for 2 hours at room temperature was then carried out. After washing in buffer, the cells were then dehydrated through increasing concentrations of ethanol (70, 95, 100% Fisher Scientific). Dehydrated Ti-64 discs were then immersed in 50% hexamethyldisilazane/50% dried ethanol for one hour, then left in hexamethyldisilazane overnight. The discs were sputter-coated with gold for 30 seconds at a current of 35 mA, and examined using the Inspect-F50 (FEI, Oregon,USA) and Philips XL 20 (Royal Philips Electronic, Eindhoven, The Netherlands) scanning electron microscopes.

The cells cultured on Ti-64 EBM and MIM implant discs were also prepared for morphological and genetic expression (ie cytoskeleton) analysis via confocal fluorescent microscopy. The cells were fixed, their actin filaments and nucleii stained and then images were taken. This was achieved by seeding cells on Ti-64 implant discs for 2 and 8 days as described above. The media was removed and the cells were washed once with PBS after which the discs were moved to new 24-well plates. The cells were fixed with 3.7% formaldehyde solution for 20 minutes at room temperature. The cells were then washed 3 times with PBS twice for five minutes. After that, 0.1% (v/v) Triton X 100 solution was added then cells were incubated for 30 minutes at room temperature and then washed 3 times again with PBS. Phalloidin-TRITC (red) (Phalloidin, Fluorescein Isothiocyanate, Sigma-Aldrich) solution was added to the cells and incubated for 30 minutes at room temperature in the dark by covering the plate in aluminium foil. The cells were again washed three times with PBS. In order to label cell nuclei, a solution of Hoescht 33342 (Thermo Scientific, Altrincham, UK) was used and

incubated for 15 minutes at room temperature in the dark. After washing again three times with PBS, the cells were ready for imaging. Images (512 x 512 size) were obtained using a Zeiss LSM 510Meta upright confocal microscope (Carl Zeiss, Oberkochen, Germany) equipped with an Achroplan 40x/0.8W objective, using pixel dwell times of 25.6µs and 34.5µs. All image analysis was performed using the Zeiss LSM Image Browser software.

2.3.4 *Statistical analysis*

All the values of the fluorescence and absorbance measurements were obtained as means and standard error. For the analysis of all data the software program Statease Design-Expert for Windows (version 6) was used. Analysis of variance (ANOVA) and independent sample T-test were used to identify the effect of surface roughness based on build orientation on cell viability. Values of $p < 0.05$ were considered to be statistically significant to the reference MIM titanium and indicated by an asterisk (*).

3. **Results**

3.1 Surface characterisation

Surface	Ra (µm)	Rq (µm)	Rp (µm)	Rv (µm)	Rt (µm)
Vertical	38	48	544	-352	896
Horizontal	18	23	56	-77	133
Inclined	45	64	324	-513	837
MIM Ref	5	7	38	-94	131

Table 2: Surface Characteristics of the EBM and MIM Ti-64 disks characterised through interferometry

Table 2 shows the results of the surface characteristics of the EBM and MIM Ti-64 discs characterised through white light interferometry. The topographic 3D views of the vertical, horizontal inclined EBM Ti-64 and a MIM Ti-64 surface used as a reference are shown with their corresponding R_a values in Figure 3. The scanning electron microscope images in Figure 4 show the surface topographies of the vertical, horizontal, inclined EBM Ti-64 parts in comparison to the reference MIM Ti-64 component. The bottom row in Figure 4 shows the micrographs at higher magnifications. Different topographies on the Ti-64 disc implants were achieved as a result of the anisotropic character of the layer by layer generation process [17]. It can be deduced from Table 2, Figure 3 and Figure 4 that the electron beam melted specimens have a generally rougher surface in terms of the R_a value than their MIM counterpart primarily due to the difference in the starting powder particle sizes used. The MIM staring powder was sub 45µm [23] whereas the EBM starting powder was sub 105µm.

Table 2 also reveals that among the EBM Ti-64 samples, the least rough surface was obtained on the horizontal orientation of the Ti-64 within EBM chamber (R_a and R_q). This is attributed to the ability of the EBM machine to melt all the powder when it is exposed to the beam source in a normal direction. On the EBM system, the actual melting and welding together of powder particles takes place on the horizontal plane which results in a beam hatching pattern of parallel groves 200µm wide. When comparing the surface topographies of the EBM horizontal and reference MIM samples, the EBM horizontal sample also had a smallest value of the maximum profile depth (R_v) also due to the complete melting of powder particles. However the presence of lines on the EBM horizontal surface which are attributed to melt tracks based on the beam hatching strategy contributed to a higher measurements of R_a and R_q.

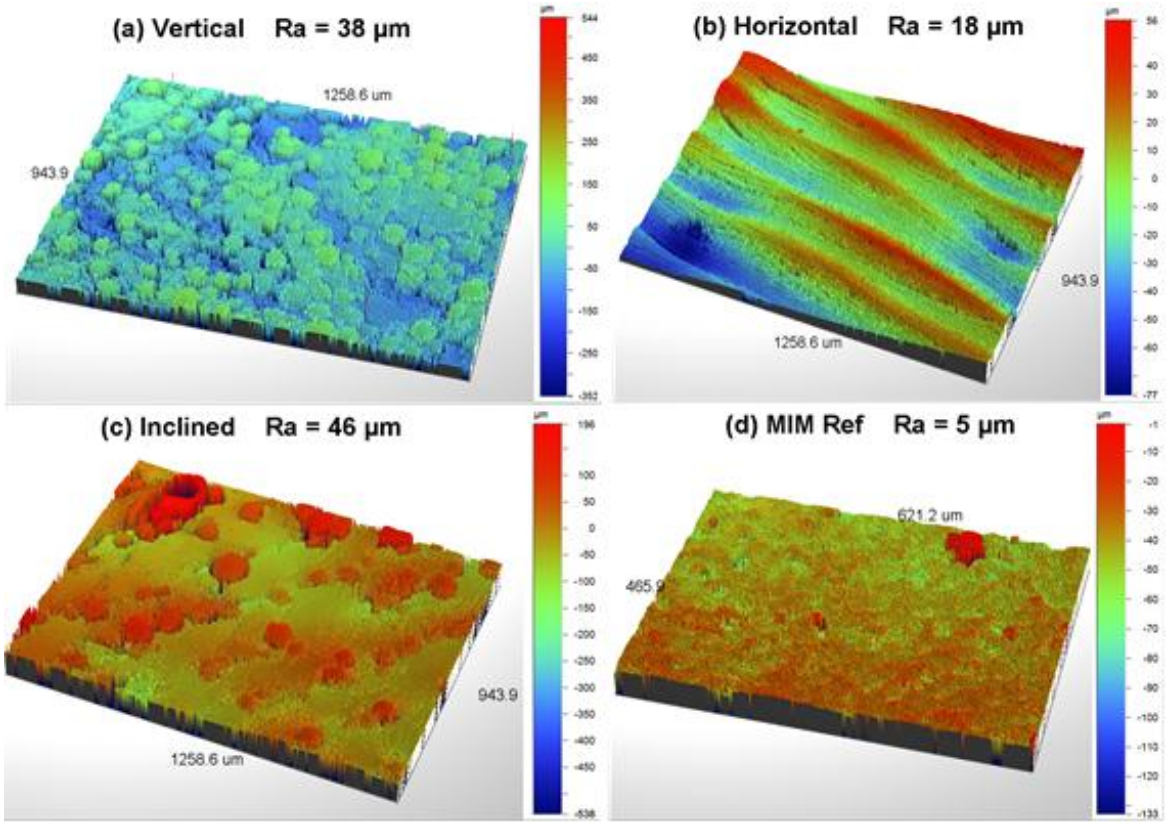

Figure 3: Topographic 3D view of EBM Ti-64 vertical, horizontal and inclined surfaces showing corresponding R_a values compared against a MIM reference sample surface

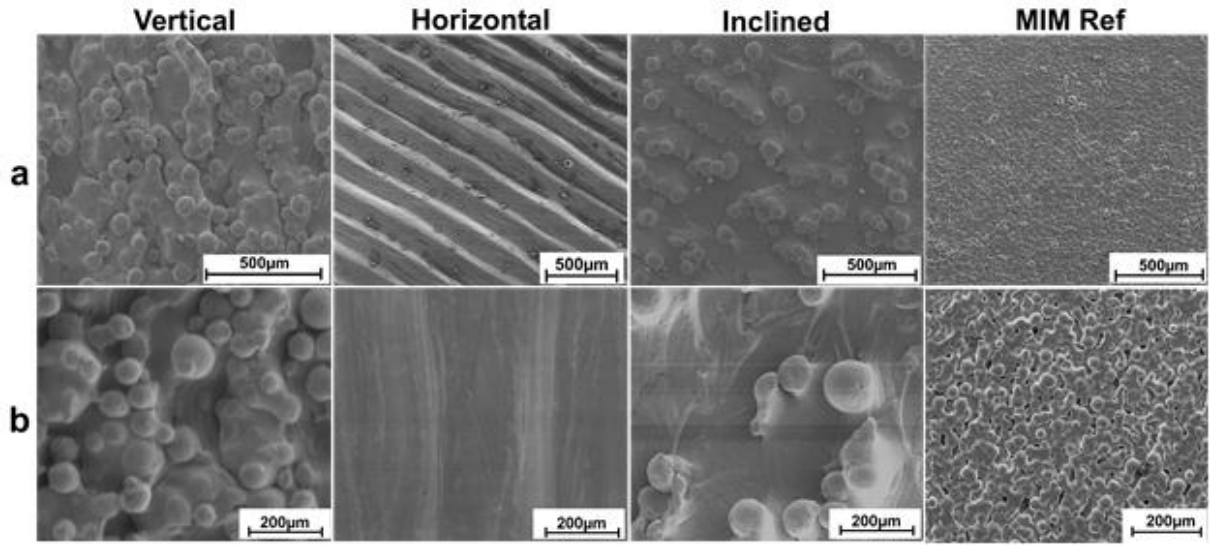

Figure 4: SEM surface topography comparing the vertical, horizontal and inclined EBM Ti-64 components. The bottom row shows the micrographs at higher magnifications

The vertical and inclined EBM surfaces are shown to have a rough profile and this is attributed to adherent unmelted powder particles. The SEM micrographs in Figure 4 and the topographic 3D views in Figure 3 confirm the presence of adherent unmelted powder. The inclination of samples in the build chamber resulted in a combination of regions of smooth completely melted powder and regions of rough morphology due to unmelted powder particles, leading to a rougher surface profile (R_a and R_q) of the inclined orientation than of the vertical where the unmelted powder particles were more densely

populated. The highest value of the maximum profile peak height (R_p) was obtained from the specimens in the vertical orientation whereas the highest maximum profile valley depth (R_v) was obtained from inclined EBM samples. It can be seen from Table 2 that R_p and R_v were considerably higher in the vertical and inclined samples than on the horizontal EBM than on the reference Ti-64 MIM surface. Overall, the highest value of the total profile height (R_t) was obtained on the vertical oriented EBM sample.

3.2 Cell proliferation and morphology

Figure 5 shows scanning electron micrographs of L929 mouse fibroblast cell attachment, growth and proliferation on vertical, horizontal, inclined EBM compared to a MIM reference Ti-64 discs. The SEM micrographs show cells that were cultured for 2 days and micrographs are also shown at a higher magnification. The attachment, growth and proliferation of cells that were cultured for 8 days are shown in Figure 6 including higher magnification micrographs.

The SEM micrographs show that the cells attached and spread well on all surfaces. The L929 cells showed typical filamentous morphology of L929 fibroblasts. It is clearly visible that the number of cells on all surfaces cultured for 8 days was higher than on surfaces cultured for 2 days and that the cells covered whole areas of all the samples after 8 days. It is expected that cells grow on biocompatible surfaces with passage of time. In comparing the EBM Ti-64 cell growth to the reference MIM sample, it was found that the cell distribution was more homogenous and cells appeared to cover more of the sample area on the MIM sample than on the EBM samples. The higher magnification micrographs of the cells cultured for 2 days show cellular filopodia interaction of the L929 cells with the EBM and MIM surfaces. Cells displayed a morphology that is expected with the L929 cell line, exhibiting cellular protrusions extending from the cellular periphery. The EBM samples showed that cells were more proliferate in deep lying regions of the rough surfaces. On the vertical and inclined EBM samples cultured for 2 days, cell growth was less on the unmelted powder particle surfaces whereas on the horizontal EBM samples, the cells grew on the top ridges of the surface during the initial attachment stage.

Figure 7 shows stained nuclei (blue) and F-actin (red) patterns of L929 cells cultured for 2 days on the EBM and MIM Ti-64 implants at two different magnifications. As it can be seen from Figure 7, the volume of cells on the MIM sample appears to be higher due to the more regular (flatter) nature of the surface topography. All the cells displayed cytoskeletal actin organisation that is consistent with L929 cells on irregular implant surfaces. The nuclei staining showed round irregular distribution which is also consistent with the EBM Ti-64 surfaces. That is, the horizontal samples showed less concentration of cells in the valley groves of the surface whereas on the vertical and inclined implants, the staining of the nuclei revealed the growth of the cells below and around the non-melted powder particles. On the reference MIM sample the nuclei were found to be well distributed on across the regular surface (see Figure 4). There were more of the flat cell morphology on the MIM reference sample than al all the EBM Ti-64 implants.

3.3 Cell Viability and cytotoxicity

Figure 8 shows the results of fluorescence measurements as a measure of the cell viability on three different orientation EBM Ti-64 disc implants and on the MIM sample after 2 and 8 days of cell incubation. After 2 days the number of cells was highest on the rougher topographies of the vertical followed by inclined specimens than on the horizontal EBM Ti-64. The number of viable cells on both the vertically and inclined oriented EBM Ti-64 were comparable to those on the reference MIM sample after 2 days. Furthermore, after 2 days of culture, a statistically significant difference ($p<0.05$) was found between vertical and reference MIM and also between horizontal EBM and reference MIM as indicated by (*).

Figure 8 also shows that the fluorescence, and therefore the number of cells increased significantly (by order of 3) after 8 days of cell culture. Similar to the number of live cells detected after 2 days of culture the highest fluorescence readings amongst the EBM Ti-64 implants were recorded on the vertical, followed by inclined and then the horizontal samples. There was a higher cell growth detected on the reference MIM Ti-64 specimen after 8 days of cell culture. There was no statistical significance between any of the measurements after 8 days. Figure 9 shows the results of the cytotoxicity measurements that were determined through measurement of the optical densities (absorbance) at the 490 nm visible wavelength. The control indicates cells grown on a well plate.

The amount of LDH released is proportional to the number of dead cells, which is quantified through a colorimetric assay by measuring the absorbance at 490 nm. The absorbance value reported in this study was calculated using the LDH released from the live cells in the Ti-64 implants medium (after they were lysed) after 2 days. Therefore a larger number of cells detected via LDH release amongst the EBM samples were detected in the horizontal Ti-64 implants, followed by the vertical and then the inclined implants. The reference MIM Ti-64 implants revealed a detection of more cells than all of the EBM implants. The results appear to contradict the findings of the cell viability studies (Figure 8). This can be attributed to the way in which cells adhere to the different surfaces. It is possible that it was easier to retrieve lysed cells from the horizontal EBM and MIM Ti-64 because the rougher vertical and inclined EBM topographies entrapped some lysed cells. This implies that the rougher vertical and inclined EBM topographies supported stronger cell orientation and alignment.

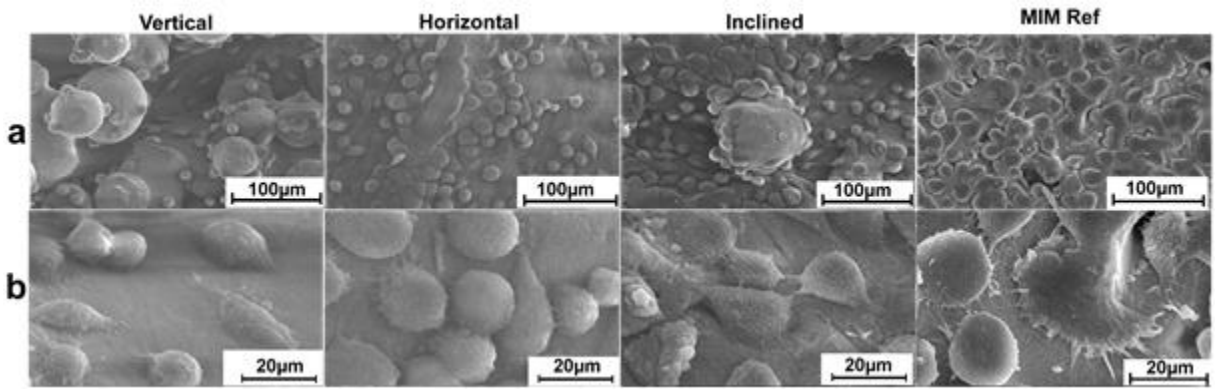

Figure 5: Scanning electron micrographs of L929 mouse fibroblast cells cultured on vertical, horizontal, vertical EBM and MIM Ref Ti-64 discs for 2 days. Micrographs are also shown at a higher magnification (b).

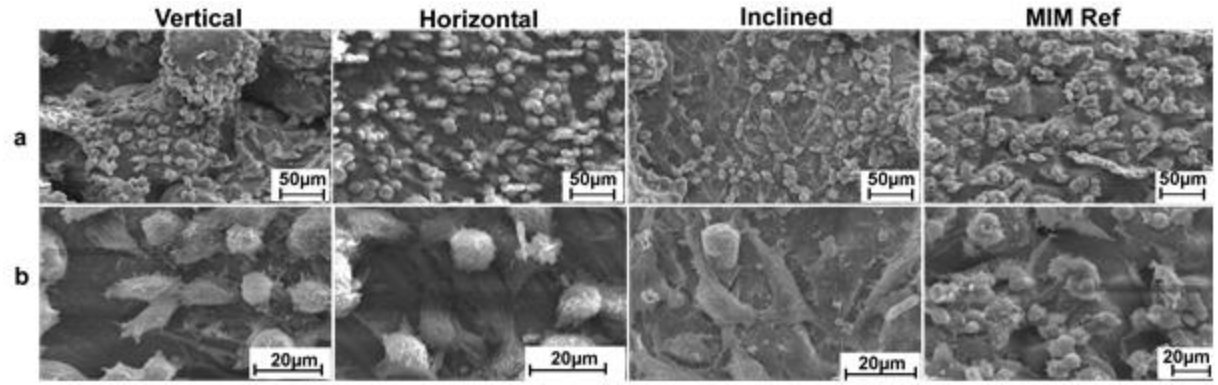

Figure 6: Scanning electron micrographs of L929 mouse fibroblast cells cultured on vertical, horizontal, vertical EBM and MIM Ref Ti-64 discs for 8 days (a). Micrographs are also shown at a higher magnification (b).

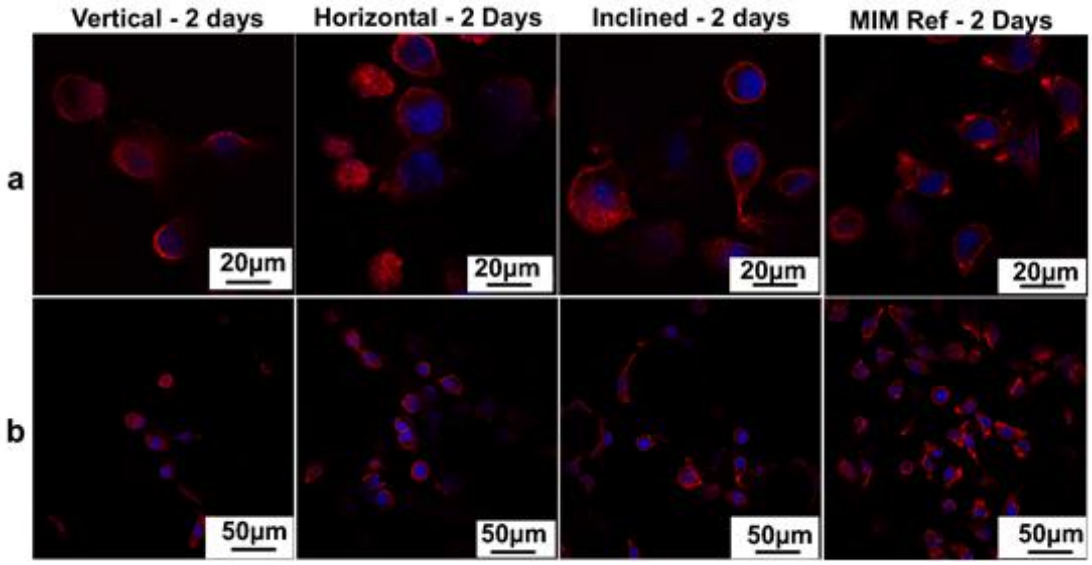

Figure 7: Stained nuclei and F-actin patterns of L929 cells cultured for 2 days on the EBM and MIM Ti-64 implants

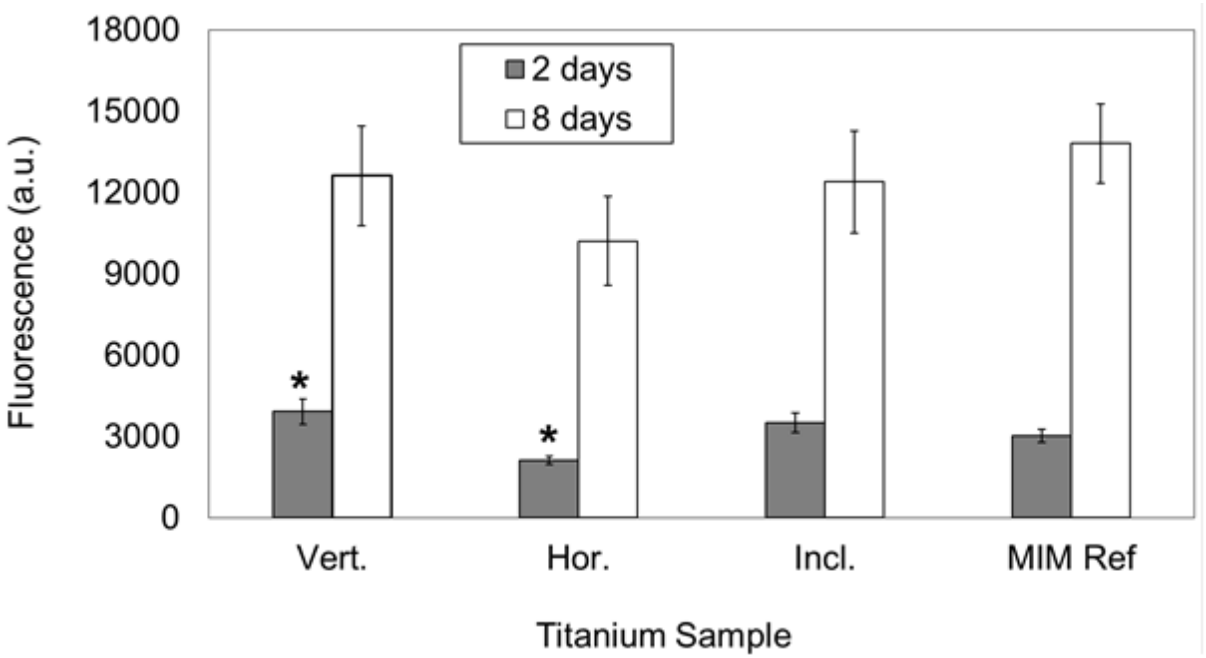

Figure 8: Cell viability on the different build orientation EBM and MIM Ti-64 disc samples (n=6) after 2 and 8 days. Fluorescence measured at 590 nm.

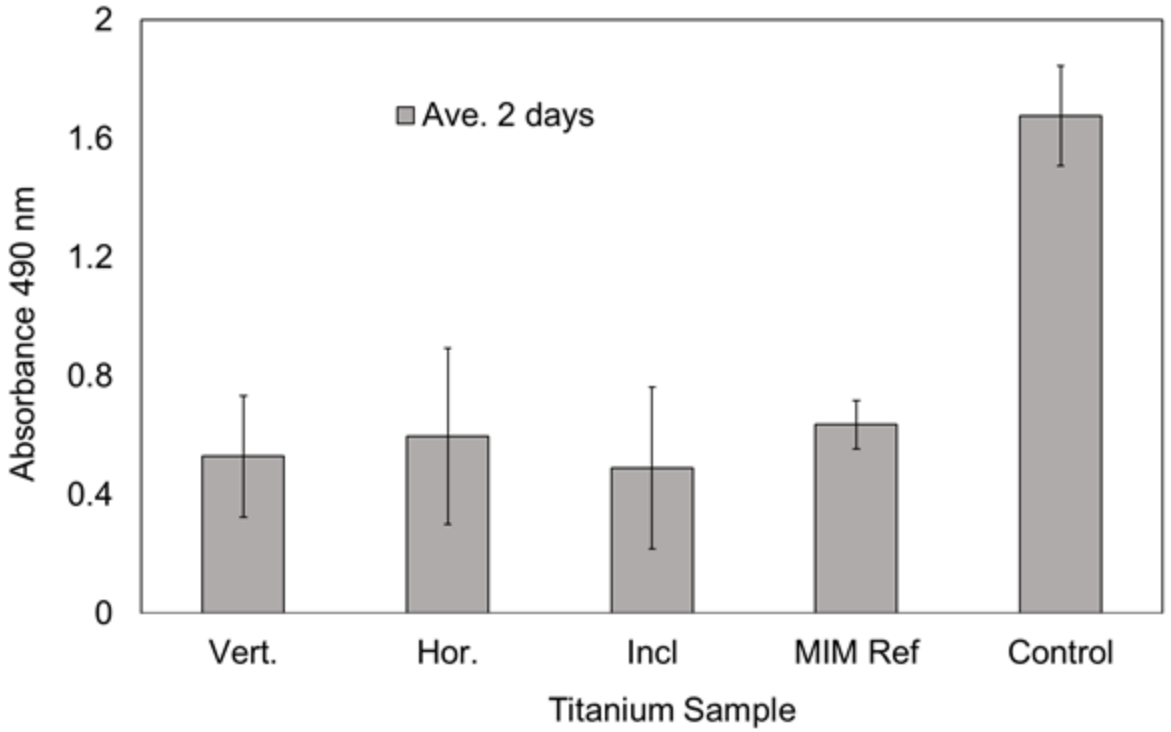

Figure 9: Cytotoxicity of EBM and MIM Ti-64 disc samples (n=6) results measured at 490 nm after 2 days incubation

4. Discussion

The results have revealed that different surface topographies can be obtained as a result of orientation in the EBM build chamber. There are various factors that are intrinsic within the EBM process which result in the different surface topographies that have been obtained in the study. It was shown that the surface roughness of the Ti-64 disc implants were in the micrometer scale. The vertical orientation roughness values outlined in Table 2 indicate that there is a larger volume of more densely populated partial melted adherent particles as a direct result of the lack of exposure to the beam. The inclined orientation values suggest that the volume of partially melted particle is reduced as can be seen from Figure 4 because beam energy per unit volume is increased. The horizontal surface had no unmelted powder particles because that is where beam energy is maximised, but there are lines and grove valleys as a result of melt tracks. The surface features have also been discussed in terms of the surface topographies which include the width, height and depth of the features. The different surface features have been shown to promote cell growth in slightly varying degrees. The results show that the surface properties affect the mass transport ability, influencing cell attachment and growth and therefore tissue regeneration on an implant's surface, even on a micrometer scale. Other surface properties such as chemical compositions can be influential but they have not been studied in this work.

The surface topography of the Ti-64 implants oriented horizontally has been shown to have the lowest cell viability after 2 and 8 days, whereas the cytocompatibility studies based on cell count revealed that the horizontal surface topography had the larger number of live cells which had been lysed. The results have not revealed any significant advantage of the MIM Ti-64 implant in comparison to EBM Ti-64 implants based on the difference of the surface topography. The growth of L929 cells on MIM reference sample is therefore comparable to the rougher EBM Ti-64 samples. Therefore, examination of the factors that affect cell growth, particularly the attachment and proliferation of cells on the Ti-64 surfaces has shown that the rough surfaces could support cell attachment and proliferation, as well as on homogeneous surface samples such as MIM Ti-64. It can, therefore, be postulated that the *in vitro* L929 responses to EBM and MIM Ti-64 are influenced by the surface property induced by orientation in the EBM build chamber. It is apparent that this difference is due to the larger specific surface area of

the EBM vertical, inclined and MIM Ti-64. Therefore build orientation and therefore the specific surface area remains an important factor of implant design in the investigation of EBM solid implants' biological performance.

5. Conclusion

In this study Ti-64 implant discs with different surface topographies were successfully built using the advanced EBM technique and then compared to a reference MIM disc. Although they all supported the attachment and proliferation of L929 fibroblast cells during our experiments, the samples with rougher surfaces (vertical and inclined) were slightly more compatible due to probably larger specific surface area than the smoother surface (horizontal). They were comparable to the reference MIM surface which was more homogeneous and had the smoothest surface roughness complemented by a high maximum depth profile. This study has demonstrated that electron beam melting can be used successfully to manufacture safe, biocompatible titanium alloy structures for use as medical devices in some applications. The process can be used in designing implants with specific surface roughnesses. The biocompatibility studies have shown how the design flexibility can be correlated with cell proliferation through the use of the EBM process as an enabling environment for the manufacture of implants with tailored surfaces based on their orientation in the build chamber. This study has shown that there may be complexities associated with EBM implants in that the cell attachment or bone ingrowth, for example, may not be uniform throughout a single Ti implant part due to part orientation in build chamber.

6. Acknowledgements

The authors sincerely thank Dr. Fatos Derguti and the staff at the Mercury Centre (University of Sheffield) for help with fabrication of the EBM Ti-64 discs and Dr. Nicola Green at the Kroto Imaging Facility (University of Sheffield) for help with acquisition of images on the fluorescent microscope. Finally, the authors would like to thank the Wellcome Trust for providing financial support through the Institutional Strategic Support Fund (ISSF) at the University of Sheffield to conduct the present research.

7. References

[1] Shibo, G.; Xuanhui, Q.; Ting, Z.; Bohua, D. Powder injection molding of Ti–6Al–4V alloy. *J. Mat. Proc. Tech.* **2006**, *173*, 310-314. doi: 10.1016/j.jmatprotec.2005.12.001.

[2] Sidambe, A.T.; Figueroa, I.A.; Hamilton, H.G.C.; Todd, I. Metal injection moulding of CP-Ti components for biomedical applications. *J. Mater. Process Tech.* **2012**, *212*, 1591-1597. doi: 10.1016/j.jmatprotec.2012.03.001.

[3] Sidambe, A. Biocompatibility of Advanced Manufactured Titanium Implants—A Review. **2014**, *7*, 8168-8188. doi: 10.3390/ma7128168.

[4] Elias, C.N.; Lima, J.H.C.; Valiev, R.; Meyers, M.A. Biomedical applications of titanium and its alloys. *JOM* **2008**, *60*, 46-49. doi: 10.1007/s11837-008-0031-1.

[5] Sidambe, A.T.; Choong, W.L.; Hamilton, H.G.C.; Todd, I. Correlation of metal injection moulded Ti6Al4V yield strength with resonance frequency (PCRT) measurements. *Mat. Sci. Eng. A-Struct.* **2013**, *568*, 220-227. doi: 10.1016/j.msea.2013.01.040.

[6] Froes, F.H. Titanium Powder Metallurgy: A Review - Part 1. *Adv. Mater. Process.* **2012**, *170*, 16-22.

[7] Froes, F.H. Titanium Powder Metallurgy: A Review - Part 2. *Adv. Mater. Process.* **2012**, *170*, 26-29.

[8] van Noort, R. The future of dental devices is digital. *Dent. Mater.* **2012**, *28*, 3-12. doi: 10.1016/j.dental.2011.10.014.

[9] Hollander, D.A.; Wirtz, T.; Walter, M.V.; Linker, R.; Schultheis, A.; Paar, O. Development of Individual Three-Dimensional Bone Substitutes Using "Selective Laser Melting". *Eur. J. Trauma* **2003**, *4*, 228-234. doi: 10.1007/s00068-003-1332-2.

[10] Haslauer, C.M.; Springer, J.C.; Harrysson, O.L.A.; Loboa, E.G.; Monteiro-Riviere, N.A.; Marcellin-Little, D.J. In vitro biocompatibility of titanium alloy discs made using direct metal fabrication. *Med. Eng. Phys.* **2010**, *32*, 645-652. doi: 10.1016/j.medengphy.2010.04.003.

[11] Murr, L.E.; Amato, K.N.; Li, S.J.; Tian, Y.X.; Cheng, X.Y.; Gaytan, S.M.; Martinez, E.; Shindo, P.W.; Medina, F.; Wicker, R.B. Microstructure and mechanical properties of open-cellular biomaterials prototypes for total knee replacement implants fabricated by electron beam

melting. *J. Mech. Behav. Biomed. Mater. 2* **2011**, *4*, 1396-1411. doi: 10.1016/j.jmbbm.2011.05.010.

[12] Ivanova, O.; Williams, C.; Campbell, T. Additive manufacturing (AM) and nanotechnology: promises and challenges. *Rapid Prototyping J.* **2013**, *19*, 353-364. doi: 10.1108/Rpj-12-2011-0127.

[13] Chahine, G.; Koike, M.; Okabe, T.; Smith, P.; Kovacevic, R. The design and production of Ti-6Al-4V ELI customized dental implants. *JOM* **2008**, *60*, 50-55. doi: 10.1007/s11837-008-0148-2.

[14] Al-Bermani, S.S.; Blackmore, M.L.; Zhang, W.; Todd, I. The Origin of Microstructural Diversity, Texture, and Mechanical Properties in Electron Beam Melted Ti-6Al-4V. *Metall. Mater. Trans. A* **2010**, *41A*, 3422-3434. doi: 10.1007/s11661-010-0397-x.

[15] Lv, J.; Jia, Z.; Li, J.; Wang, Y.; Yang, J.; Xiu, P.; Zhang, K.; Cai, H.; Liu, Z. Electron Beam Melting Fabrication of Porous Ti6Al4V Scaffolds: Cytocompatibility and Osteogenesis. **2015**, n/a-n/a. doi: 10.1002/adem.201400508.

[16] Kearns, V.R.; McMurray, R.J.; Dalby, M.J. 7 - Biomaterial surface topography to control cellular response: technologies, cell behaviour and biomedical applications. In *Surface Modification of Biomaterials*; Williams, R., Ed. Woodhead Publishing: 2011; pp. 169-201. doi: http://dx.doi.org/10.1533/9780857090768.1.169.

[17] Ponader, S.; Vairaktaris, E.; Heinl, P.; Wilmowsky, C.v.; Rottmair, A.; Körner, C.; Singer, R.F.; Holst, S.; Schlegel, K.A.; Neukam, F.W.; Nkenke, E. Effects of topographical surface modifications of electron beam melted Ti-6Al-4V titanium on human fetal osteoblasts. *J. Bio. Mater. Res. A* **2008**, *84A*, 1111-1119. doi: 10.1002/jbm.a.31540.

[18] Chen, H.; Sago, A.; West, S.; Farina, J.; Eckert, J.; Broadley, M. Biocompatibility of metal injection molded versus wrought ASTM F562 (MP35N) and ASTM F1537 (CCM) cobalt alloys. *Bio-Med. Mater. Eng.* **2011**, *21*, 1-7. doi: 10.3233/BME-2011-0652.

[19] Ponader, S.; Von Wilmowsky, C.; Widenmayer, M.; Lutz, R.; Heinl, P.; Körner, C.; Singer, R.F.; Nkenke, E.; Neukam, F.W.; Schlegel, K.A. In vivo performance of selective electron beam-melted Ti-6Al-4V structures. *J. Bio. Mater. Res. A.* **2009**, *92*, 56-62. doi: 10.1002/jbm.a.32337.

[20] Thomsen, P.; Malmström, J.; Emanuelsson, L.; René, M.; Snis, A. Electron beam-melted, free-form-fabricated titanium alloy implants: Material surface characterization and early bone response in rabbits. *J. Biomed. Mater. Res. B* **2009**, *90B*, 35-44. doi: 10.1002/jbm.b.31250.

[21] Li, X.; Feng, Y.F.; Wang, C.T.; Li, G.C.; Lei, W.; Zhang, Z.Y.; Wang, L. Evaluation of Biological Properties of Electron Beam Melted Ti6Al4V Implant with Biomimetic Coating In Vitro and In Vivo. *Plos One* **2012**, *7, e52049*. doi: 10.1371/journal.pone.0052049.

[22] Palmquist, A.; Snis, A.; Emanuelsson, L.; Browne, M.; Thomsen, P. Long-term biocompatibility and osseointegration of electron beam melted, free-form–fabricated solid and porous titanium alloy: Experimental studies in sheep. *J. Bio. Mater. App.* **2013**, *27*, 1003-1016. doi: 10.1177/0885328211431857.

[23] Sidambe, A.; Todd, I.; Hatton, P., Effect of Processing Parameters on the Properties of Metal Injection Moulded Titanium Dental Implants. In *Materials Science Forum*, 2015.

[24] ISO 10993-5:2009, Biological evaluation of medical devices. Part 5: Tests for in vitro cytotoxicity, International Organisation for Standardisation (ISO), Geneva, **2009**.

[25] Samal, S.K.; Dash, M.; Declercq, H.A.; Gheysens, T.; Dendooven, J.; Van Der Voort, P.; Cornelissen, R.; Dubruel, P.; Kaplan, D.L. Enzymatic mineralization of silk scaffolds. **2014**, *14*, 991-1003. doi: 10.1002/mabi.201300513.

[26] Promega_Corporation CytoTox 96® Non-Radioactive Cytotoxicity Assay Technical Bulletin. Available online: https://www.promega.co.uk/resources/protocols/technical-bulletins/0/cytotox-96-non-radioactive-cytotoxicity-assay-protocol/ (19 May 2015),